Lattice effects in crystal evaporation



1994 J. Phys. A: Math. Gen. 27 1859

(http://iopscience.iop.org/0305-4470/27/6/013)

J. Phys. A: Math. Gen. 27 (1994) 1859–1876. Printed in the UK

# Lattice effects in crystal evaporation

I Pagonabarraga†, J Villain, I Elkinani and M B Gordon

DRFMC/SPSMS/MDN, Centre d'Etudes Nucléaires de Grenoble, 85X, F-38041 Grenoble, Cedex, France

Received 20 July 1993

**Abstract.** We study the dynamics of a stepped crystal surface during evaporation, using the classical model of Burton, Cabrera and Frank, in which the dynamics of the surface is represented as a motion of parallel, monatomic steps. The validity of the continuum approximation treated by Frank is checked against numerical calculations and simple, qualitative arguments. The continuum approximation is found to suffer from limitations related, in particular, to the existence of angular points. These limitations are often related to the adatom detachment rate which is higher on the lower side of each step than on the upper side ('Schwoebel effect').

## 1. Introduction

The study of the dynamics of a crystal surface under non-equilibrium conditions is an old subject, the interest of which was renewed in the last years due to modern experimental techniques, such as electron reflection microscopy [1, 2], which allow a more detailed observation of dynamic phenomena of the surfaces both during evaporation and growth. Moreover, equilibrium is practically never reached, and even a surface which is apparently at equilibrium on a certain length-scale, will present non-equilibrium shapes at larger length-scales. Therefore, it is of interest to understand how these features can be formed, either during growth or during annealing.

Burton, Cabrera and Frank [3] (BCF) have developed a simple theory to describe the growth of a stepped, dislocation-free crystal surface. They wrote equations of motion for the steps. The purpose of the present article is to solve these equations for special cases corresponding to a given initial profile of the surface.

When trying to solve the BCF equations, a possible approach is to make the continuum approximation. Then, as will be seen in section 2, it is possible to use a theorem discovered by Frank [4]. However, the continuum approximation is questionable if the slope of the surface is discontinuous. For that reason, the present work is focussed on the evaporation of surfaces which initially contain corners (figure 1($a$)).

Only evaporation will be considered here, in order to avoid problems due to nucleation of new terraces during growth. One can also notice that in situ study of surface dynamics is more easily performed under evaporation than under growth conditions [1, 2]. In this paper we investigate, within the BCF theory, the evaporation of a defect-free surface made of parallel, but not equidistant, steps. Our main motivation is to test, in particular instances, the validity of the continuum approximation developed by Frank [4]. The continuum

† Current address: Department de Física Fonamental, Universitat de Barcelona, Av. Diagonal 647, 08028 Barcelona, Spain.

0305-4470/94/061859+18$19.50  

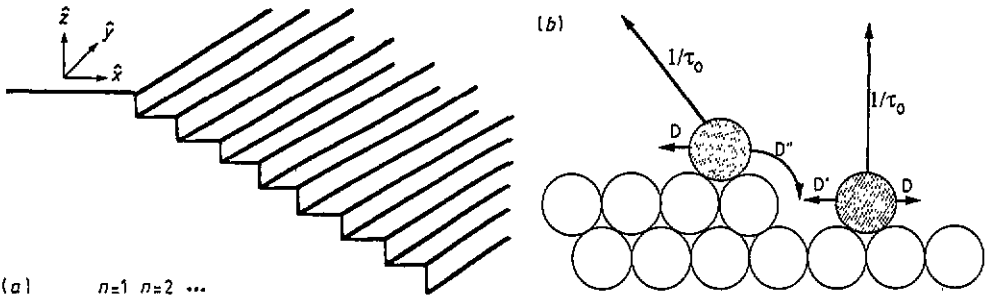


**Figure 1.** (*a*) Profile of a crystal surface made of two semi-infinite half planes. The left-side surface corresponds to a high symmetry plane. (*b*) Diagram of the movement of adatoms on terraces, showing the probability of each event. Schwoebel effect is taken into account through the coefficients $D'$ and $D''$.

approximation will be shown to fail when curvature changes abruptly at some place on the surface. In the original BCF paper, atoms detaching from a step were assumed to be emitted with equal probability from the upper and from the lower terrace. This will be called the *symmetric case*. However, as noticed by Ehrlich [5], a step may be partially rather than totally absorbing. Generally, one side is more absorbing than the other [6]. This is known as Schwoebel effect.

We will consider solid surfaces made of parallel steps. The structure of the surface at time $t$ is fully characterized by the positions $x_n(t)$ of the successive steps labelled by the index $n = 1, 2, \ldots$, as shown in figure 1(*a*). The functions $x_n(t)$ satisfy the following equation, which follows from the BCF theory, appropriately modified to take into account the Schwoebel effect:

$$\dot{x}_n = -\varphi_l(x_n - x_{n-1}) - \varphi_r(x_{n+1} - x_n). \tag{1.1}$$

The expressions of $\varphi_l(l)$ and $\varphi_r(l)$ are derived in [7] and, for completeness, briefly re-derived in appendix A. The first one,

$$\varphi_l(l) = (\rho_0 - F\tau_0)\frac{\cosh(\kappa l) - 1 + \frac{\kappa D}{D'}\sinh(\kappa l)}{\left(1 + \frac{\kappa^2 D^2}{D'D''}\right)\sinh(\kappa l) + \left(\frac{\kappa D}{D'} + \frac{\kappa D}{D''}\right)\cosh(\kappa l)}\kappa D \tag{1.2}$$

gives the net flux of outgoing adatoms from a step to the upper terrace, and

$$\varphi_r(l) = (\rho_0 - F\tau_0)\frac{\cosh(\kappa l) - 1 + \frac{\kappa D}{D''}\sinh(\kappa l)}{\left(1 + \frac{\kappa^2 D^2}{D'D''}\right)\sinh(\kappa l) + \left(\frac{\kappa D}{D'} + \frac{\kappa D}{D''}\right)\cosh(\kappa l)}\kappa D \tag{1.3}$$

is the net flux of outgoing adatoms from a step to the lower terrace. In these expressions, $\rho_0$ is the equilibrium density of adatoms on the high-symmetry surface at the appropriate temperature and vapour pressure, $D$ is the surface diffusion constant of adatoms and $1/\tau_0$ is the evaporation probability of an adatom per unit time. $F$ is zero in the cases addressed here, but it would be the beam intensity in the case of growth by molecular beam epitaxy. $D'$ is the unit time probability of an adatom to stick to a step when it is just beside the step, and $D''$ is the unit time probability of an adatom to stick to a step when it is just above that step (figure 1(*b*)). The situation where $D' \neq D$ and $D'' \neq D$ will correspond to situations in which the sticking probability of adatoms to steps will depend on the terrace towards which they move. More specifically, we will call normal Schwoebel effect when particles

mainly move towards the upper terrace, $D'' \ll D$, while the situation in which particles move towards the lower terrace will be named inverse Schwoebel effect. Finally,

$$\kappa = \frac{1}{\sqrt{D\tau_0}} \tag{1.4}$$

is the reciprocal of the average distance on which an adatom would diffuse on an infinite terrace before evaporating. This distance is always much larger than the interatomic spacing, taken to be the length unit throughout this work, while the time an adatom needs to diffuse along the interatomic distance is the unit time. Normal Schwoebel effect is known to produce instabilities during evaporation [8], but the present study is restricted to cases where no such instability occurs.

As seen from (1.2) and (1.3), $\varphi_l(l)$ and $\varphi_r(l)$ are proportional to $l$ for small $l$ and constant for large $l$. In the symmetric case one has $D' = D'' = D$ and, since $\kappa \ll 1$, (1.2) and (1.3) reduce to the BCF formula

$$\varphi_l(l) = \varphi_r(l) = \varphi(l) = D\kappa(F\tau_0 - \rho_0)\tanh\left(\frac{\kappa l}{2}\right). \tag{1.5}$$

The conditions of applicability of the BCF theory, which implies the stability of the step flow regime, are the following.

(i) No dislocations should be present. Generally this implies that only a small part of the surface is observed, e.g. 0.01 cm × 0.01 cm for Si wafers [1].
(ii) No surface vacancies should be formed on terraces. This implies that the temperature should not exceed a certain threshold, e.g. 1200K for Si(001) [9], although much higher for Si(111) [10].
(iii) The vicinal orientation should be stable with respect to facet formation.
(iv) The steps should not undergo instabilities, such as the one discovered by Bales and Zangwill [7] in the case of growth.

In the next section, the continuum approximation of (1.1) will be introduced and exploited. We will then focus our attention on the evaporation of a surface limited initially by two semi-infinite half planes as sketched in figure 1(*a*). One of them is assumed to be a high-symmetry surface and the other one is made of parallel steps. In section 3, the long-time behaviour of the solution of (1.1) will be derived analytically. In section 4, exact solutions will be derived for approximations of (1.1). Numerical solutions of (1.1) will be presented in section 5 and will be compared with the continuum approximation. Finally, more complicated initial profiles will be investigated in section 6, namely a periodic surface with grooves. In the discussion we summarize our main results, and technical details are worked out in the appendices.

## 2. The continuum model and Frank construction

In the continuum approximation, the step position $x_n$ is regarded as a continuous and generally differentiable function of the local surface height $-n$, also considered as a continuous variable $z$. Therefore, $x_n \to x(-z)$. Moreover, introducing the derivatives $x' = -\partial x/\partial z$, $x'' = \partial^2 x/\partial z^2$ etc, and $\varphi'(x') = \partial\varphi(x')/\partial x'$, and assuming $x'''$ and the further derivatives to be small, one can rewrite (1.1) as

$$\dot{x} = -2\phi(x') + \frac{x''}{2}\psi'(x') - \frac{x'''}{3}\phi'(x') - \frac{x''^2}{4}\phi''(x') \tag{2.1}$$

where

$$\phi(x') = \frac{\varphi_l(-x') + \varphi_r(-x')}{2} \tag{2.2}$$

$$\psi(x') = \varphi_l(-x') - \varphi_r(-x') \tag{2.3}$$

and $\varphi'$ and $\varphi''$ are the derivatives of $\varphi$.

In this section, we consider the approximation obtained by keeping only the first term in (2.1),

$$\dot{x} = -2\phi(x'). \tag{2.4}$$

This approximation will be called the continuum approximation. It clearly fails near a corner, when $x''$ is infinite. Moreover, it may be expected to be better when there is no Schwoebel effect, since then the second term of the right-hand side of equation (2.1) vanishes according to (2.3).

Equation (2.4) may alternatively be written as a relation between $z' = (\delta z/\delta x)_t = 1/(\partial x/\partial z)_t = -x'$ and $\dot{z} = (\partial x/\partial z)_x = \dot{x}/x'$:

$$\dot{z} = 2z'\phi(1/z'). \tag{2.5}$$

From this expression one can deduce the decay rate $v$ of the surface at a point characterized by a direction vector $\vec{n} = (n_x, 0, n_z)$, with $n_x = -1/\sqrt{1+x'^2}$. Due to the geometry, the decay rate is given by $v \equiv \dot{z}\, n_z = \dot{x}\, n_x$, so that

$$v = -2\frac{\phi(x')}{\sqrt{1+x'^2}} \equiv f(n). \tag{2.6}$$

This equation shows that in the continuum limit the decay rate of the surface depends only on its local orientation. The problem of the decay or growth of a surface when its velocity is a function of the orientation has been investigated by Frank [4]. Frank proved that the points at the surface with a given normal orientation move on straight lines. Let us consider the initial profile of figure 1($a$). For a velocity given by equation (2.6), we can draw the polar plot $\Gamma$ of the inverse of the velocity, as is shown in figure 2. From the curve ($\Gamma$) we can deduce the further evolution of the profile. If we take a point $P$ of the crystal where the normal is $n$, it determines a point $M$ of ($\Gamma$) through $OM//n$. Then Frank's theorem states that the point $P$ moves on a straight line parallel to the normal $n'$ to ($\Gamma$) at $M$. We will come back to this property later on.

In order to test the validity of the continuum approximation, let us consider the initial profile of figure 1($a$), such that all initial terraces have the same width except the first one. If there is a total normal Schwoebel effect such that there is no interaction between a step and its upper terrace, that is $\varphi_l(l) = 0$, then all steps will move at the same constant velocity, and therefore terrace widths will remain constant. In the other case, the interaction of the second step with a different one will induce a modification in the step velocity, and then the velocity of the steps will change in time and will be different from one to another. The continuum approximation is not sensitive to this qualitatively different behaviour induced by the Schwoebel effect. From equation (2.2), one sees that the function $\phi(x)$ does not change qualitatively whether $\varphi_l(-x')$ is zero or not. This effect will be studied quantitatively in the next section.

## 3. Upper ledges at long times

We are now concerned with the evolution of the simple profile already considered in section 2. At the beginning, the distances $l_1, l_2, \ldots$ are finite and equal. It will be shown self-

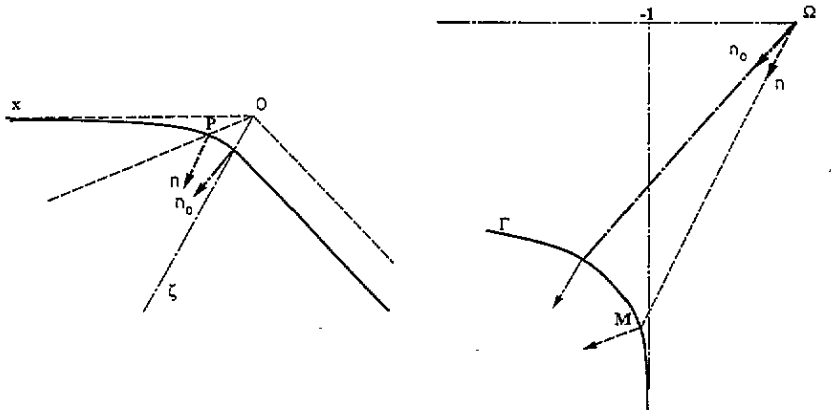


**Figure 2.** Frank's construction: left-hand part: cross section of the initial crystal (dashed curve) and of the actual one (full curve); right-hand part: the surface generated by the point $M$ defined by $\Omega M = n/v(n)$ . The point $P$ of the crystal surface where the normal is $n$ moves on the dotted straight line, parallel to the normal to $\Gamma$ at $M$. On the left-hand side of the dotted line, the crystal is planar and parallel to its original orientation. Only the useful part of the curve of $M$ has been shown. Note the presence of a point $M_\infty$ at infinity. It corresponds to $l \to \infty$ and its abcissa is $-1$, corresponding to the formula $\Omega M = -(1, l)/\varphi(l)$, where $\varphi$ is given by (1.5).

consistently that the distances go to infinity for long times. We take this as an ansatz to be proved later. For large values of $l$, equations (1.2) and (1.3) read

$$\varphi_l(l) = \Delta(A' - 2e^{-\kappa l} + C'e^{-2\kappa l}) \tag{3.1}$$

$$\varphi_r(l) = \Delta(A'' - 2e^{-\kappa l} + C''e^{-2\kappa l}) \tag{3.2}$$

where $\Delta$, $A'$, $A''$, $C'$ and $C''$ are given in appendix A. It is necessary to go to second order in $\exp(-\kappa l)$ because, when $D''$ goes to zero, $A''$ and $C''$ go to infinity while $\Delta$ goes to zero. A similar effect takes place when $D' = 0$.

From (1.1), one obtains

$$\dot{l}_n = \dot{x}_{n+1} - \dot{x}_n = -\varphi_l(l_n) - \varphi_r(l_{n+1}) + \varphi_l(l_{n-1}) + \varphi_r(l_n). \tag{3.3}$$

Combining equation (3.3) with (3.1) and (3.2), one obtains for $n > 1$

$$\dot{l}_n = \Delta\left(2e^{-\kappa l_{n+1}} - 2e^{-\kappa l_{n-1}} - C'e^{-2\kappa l_n} + C'e^{-2\kappa l_{n-1}} - C''e^{-2\kappa l_{n+1}} + C''e^{-2\kappa l_n}\right) \tag{3.4}$$

and for $n = 1$:

$$\dot{l}_1 = \Delta\left(2e^{-\kappa l_2} + (C'' - C')e^{-2\kappa l_1} - C''e^{-2\kappa l_2}\right). \tag{3.5}$$

If $C'$ and $C''$ are finite, the terms in $\exp(-2\kappa l)$ may be neglected in (3.5) for large $l$. Then these equations turn out to have solutions of the form

$$l_n(t) = \frac{1}{\kappa}\ln(B_n t) \tag{3.6}$$

Indeed, insertion of (3.6) into (3.4) yields

$$\frac{1}{B_{n+1}} = \frac{1}{B_{n-1}} + \frac{1}{2\Delta\kappa} \tag{3.7}$$

while relations (3.6) and (3.5) yield

$$\frac{1}{B_2} = \frac{1}{2\Delta\kappa}. \tag{3.8}$$

From (3.7) and (3.8) one deduces

$$\frac{1}{B_{2n}} = \frac{n}{2\kappa\Delta} \tag{3.9}$$

$$\frac{1}{B_{2n+1}} = \frac{1}{B_1} + \frac{n}{2\kappa\Delta}. \tag{3.10}$$

The numerical solution (section 5) shows that the correct solution is the most symmetrical one, namely $B_1 = 4\kappa\Delta$, so that

$$l_n(t) \simeq \frac{1}{\kappa} \ln\left(\frac{t}{n}\right). \tag{3.11}$$

Under total normal Schwoebel effect $D'' = 0$, then $\varphi_l = 0$, as seen from (1.2). Then it follows from (3.3) that $\dot{l}_n = -\varphi_l(l_{n+1}) + \varphi_l(l_n)$ and, if all $l_n$'s are equal at the beginning, they remain equal, as expected. If total inverse Schwoebel effect is considered, $D' = 0$, then $\varphi_r = 0$ as seen from (1.3), and for $\kappa l >> 1$ and $\kappa D < D''$:

$$\varphi_l(l) = (\rho_0 - F\tau_0)\tanh(\kappa l) \simeq (\rho_0 - F\tau_0)(1 - 2e^{\kappa l}). \tag{3.12}$$

In this case, expression (3.3) reduces to

$$\dot{l}_n = -\varphi_l(l_n) + \varphi_l(l_{n-1}) \tag{3.13}$$

which has a solution similar to equation (3.11)

$$l_n(t) = \frac{1}{2\kappa} \ln\left(\frac{t}{n}\right). \tag{3.14}$$

These logarithmic solutions correspond to a self-similar shape of the surface, since $l_{\alpha n}(\alpha t) = l_n(t)$ for any value of the parameter $\alpha$.

## 4. Piecewise-linear approximation

### *4.1. The approximation*

In this section we are interested in the evolution of the same profile as the one considered in the previous section, but we will focus our attention on the short-time evolution. We are again interested in solving equations (1.1) subject to the initial conditions (figure 1(*a*))

$$\begin{aligned} x_n - x_{n-1} &= l(0) \qquad n > 1 \\ x_1 - x_0 &= \infty \end{aligned} \tag{4.1}$$

with $l(0) < 2/\kappa$, so that the saturation regime has not been reached. Otherwise, the result of the previous section would apply.

In order to solve the evolution equations, we will take advantage of the form of the hyperbolic tangent, which is approximated by the piecewise-linear function

$$\varphi(\xi) = \begin{cases} \xi & \xi \leqslant 1 \\ 1 & \xi \geqslant 1 \end{cases}. \tag{4.2}$$

We will study the evolution of the initial profile equation (4.1) within the piecewise-linear approximation equation (4.2) in both the symmetric model and under total inverse Schwoebel effect.

*4.2. Symmetric model*

In this case, when all $l_n$'s are smaller than $1/\kappa$, using the form of our initial conditions (4.1), equations (1.1) read

$$\begin{aligned} \dot{x}_1 &= -\frac{A\kappa^2}{2}(x_2 - x_1) - A\kappa \\ \dot{x}_n &= -\frac{A\kappa^2}{2}(x_{n+1} - x_{n-1}) \qquad n > 1 \end{aligned} \tag{4.3}$$

where $A \equiv D(\rho_0 - F\tau_0)$. As usual, it is convenient to rewrite the evolution equations in terms of the step widths,

$$\begin{aligned} \dot{l}_1(t) &= -\frac{A\kappa^2}{2} l_2 + A\kappa \\ \dot{l}_n(t) &= \frac{A\kappa^2}{2}(l_{n-1} - l_{n+1}) \qquad n > 1. \end{aligned} \tag{4.4}$$

The solution of equations (4.4), as derived in appendix B, is of the form

$$\begin{aligned} l_{2n}(t) &= \frac{2}{\kappa} - \left[ J_0(A\kappa^2 t) + J_{2n}(A\kappa^2 t) + 2\sum_{i=1}^{n-1} J_{2i}(A\kappa^2 t) \right] \left( \frac{2}{\kappa} - l(0) \right) \\ l_{2n+1}(t) &= l_1(A\kappa^2 t) - \left[ J_1(A\kappa^2 t) + J_{2n+1}(A\kappa^2 t) \right. \\ &\qquad \left. + \sum_{i=1}^{n-1} J_{2i+1}(A\kappa^2 t) \right] \left( \frac{2}{\kappa} - l(0) \right) \qquad n \geqslant 1 \\ l_1(t) &= l(0) + \left[ J_1(A\kappa^2 t) + 2\sum_{i=1}^{\infty} J_{2i+1}(A\kappa^2 t) \right] \left( \frac{2}{\kappa} - l(0) \right). \end{aligned} \tag{4.5}$$

This solution shows that at the beginning the first step moves faster than the others, and the rest of the steps move progressively faster.

However, the validity of equation (4.5) is restricted by the fact that in equation (4.3) we have assumed all $l_n$'s to be smaller than $1/\kappa$. Thus, when the width of one step surpasses the characteristic length $2/\kappa$, this solution breaks down. The first step to fulfill this requirement is the first step, $l_1$, for a time $t \sim 2.65/A\kappa^2$. At longer times, (4.5) does not apply.

*4.3. Total inverse Schwoebel effect*

The piecewise-linear approximation will now be applied to the case $\varphi_r = 0$ within the piecewise-linear approximation. Taking the initial conditions given by equation (4.1), as $\kappa D \ll D''$, the evolution equations read, at least for small times,

$$\begin{aligned} \dot{x}_1 &= -A\kappa \\ \dot{x}_n &= -A\kappa^2(x_n - x_{x-1}) \qquad n \geqslant 2. \end{aligned} \tag{4.6}$$

In terms of the widths, one can rewrite these equations as

$$\begin{aligned} \dot{l}_1 &= A\kappa(1 - \kappa l_1) \\ \dot{l}_n &= A\kappa^2(l_{n-1} - l_n) \qquad n \geqslant 2 \end{aligned} \tag{4.7}$$

which, using as initial conditions equations (4.1), has a solution of the form

$$l_n(t) = \frac{1}{\kappa} - \left[ \frac{1}{\kappa} - l(0) \right] e^{-A\kappa^2 t} \sum_{p=1}^{n-1} \frac{(A\kappa^2 t)^p}{p!}. \tag{4.8}$$

In contrast with equation (4.5), this solution turns out to be valid for all times, because $l_n(t) < 1/\kappa$ for all $t$ and $n$, and therefore the regime of the previous section, valid in the symmetric model, is never achieved in the completely asymmetric one. However, its behaviour is qualitatively similar to the symmetric model. At short times the first step begins to move faster, while the others move at the same speed. After some time, the second step increases its velocity, separates from the following steps and approximates the first step, and so on. This behaviour is easily seen studying the difference between the width of two adjacent steps, $l_n - l_{n-1}$. This difference shows a maximum at time $t = n$. However, the height of the peak decreases with increasing $n$, which means that this effect decreases quantitatively with $n$.

## 5. Numerical results

The nonlinear character of the evolution of the crystal shape, as shown by equation (1.1), makes it impossible to find a general analytic solution of the shape as a function of time. In the previous sections we have found such analytic expressions in different asymptotic limits. However, in order to study the evolution of the profile at any time, it is necessary to carry out a numerical study of the system (1.1). The results will enable us to check the different approximations introduced so far, both in the continuum and in the discrete cases.

We have solved the differential set of equations (1.1) corresponding to the discrete model in the symmetric case, and initial conditions given by equation (4.1). We have used a fourth-order Runge–Kutta algorithm [11]. We have considered a set of 200 steps. The neighbouring left-side step to our first step is considered to be at infinity. The rightmost one is assumed to move at constant speed, which is our boundary condition and means that the results are obtained in a reference system which moves with the initial slope of the steps. This boundary condition means that the terraces at the right of the last one have not changed their width significantly. This will be true only for a certain time scale. As soon as the width of the rightmost terrace begins to evolve, our solution is wrong. From the analytic results of the previous sections, it may be argued that at $t \neq 0$ all terraces change their width. However, this change is extremely small and, as explained in the previous subsection, only the first ones change significantly, so that it takes some time until the terraces at the bottom change their width appreciably. This fact gives us an easy way to check the validity of the solution. It turns out that all relevant features, at least for the first terraces, take place during the time scale on which the numerical solutions subject to our boundary condition are valid. However, the numerical study at very short times is obscured by the discrete time step.

The differential equations are solved for different values of the initial width, $l(0)$, as well as different time steps, checking the stability of the solution against computational artifacts.

Figure 3 shows the profile at different times. Due to the fast increase in the width of the first steps with respect to the other steps, it is necessary to choose two different length scales in the vertical and horizontal axes. In the vertical axis we take the step height as the unit length, while in the horizontal axis $\kappa^{-1}$ is considered to be the unit length. This is the reason why the initial profile appears as an almost vertical straight line. Moreover, $2A\kappa^2$ is the unit time throughout the numerical calculations. The curves are plotted every nine time steps, which corresponds to a plot every $\Delta t = 0.01$.

We have also studied the behaviour of the surface at intermediate times. In this regime the numerical solution agrees with the expressions (3.6) in the symmetric model, and (3.14) in the total inverse Schwoebel model, supporting the symmetry argument we have employed

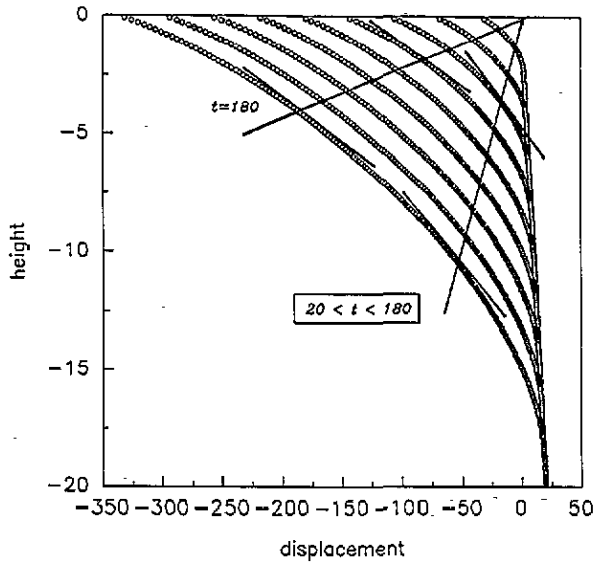


**Figure 3.** Snapshots of the evolution of the initial profile shown in figure 1(*a*) in the symmetric case. Profiles are drawn every 20 time units defined in the text. Two different scales have been chosen in the axes, as explained in the text. The profile in the discrete symmetric case is shown to be in agreement with Frank's construction. Two equal slopes at different times are seen to be joined by a straight line, and different straight lines converge at 0, the angular point at t=0.

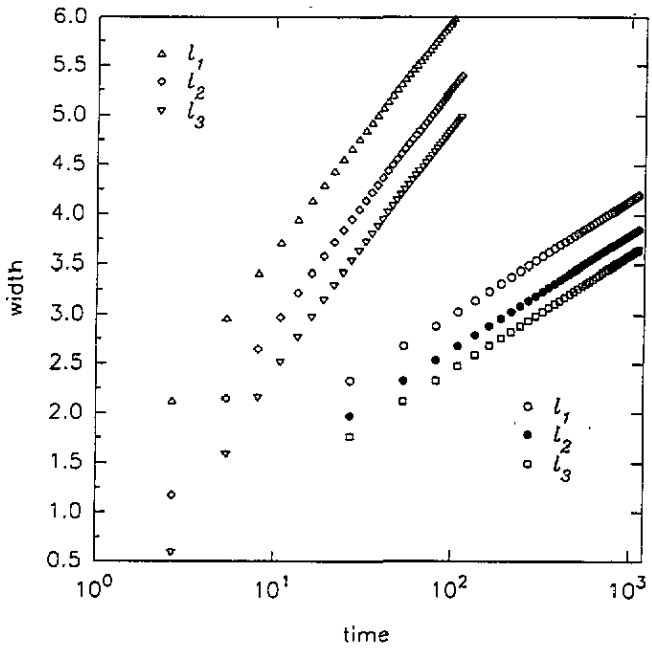


**Figure 4.** Width of the three first terraces as a function of time at long times. △, ◇ and ▽ correspond to the symmetric case, while ○, ● and □ correspond to the total inverse Schwoebel effect. The logarithmic behaviour, the prefactor and the constant are recovered in both cases. The 1/2 difference in the slope is easily appreciated.

in order to derive such equations. In figure 4 we show the width of the first three terraces as a function of time, and both the logarithmic dependence and the numerical factors are recovered exactly after a short transient in both models. The difference in the slope is easily appreciated. This good matching with the analytic predictions is again in agreement with the idea that the solution (4.5) is valid for short times, but that the saturation regime is achieved in a few time units (in the above-mentioned units).

We can compare the shape of the discrete model with the predictions of the continuum approximation. In figure 3 we have checked the validity of Frank's construction for the discrete model. We find that all lines joining points of the crystal surface, where the slope has a given value at different times, meet at a point $O$, which turns out to be the angular point at $t = 0$. Thus all shapes are homothetic of a particular one, and the homothety centre is $O$.

Finally, in figure 5 the self-similarity of the profile is checked. Neglecting a short transient, one observes a perfect scaling of the whole profile. The continuum model predicts three scaling regions, corresponding to the two initial straight lines and the part of the profile that, due to the dynamics, has deviated significantly from the other two. Therefore, two different crossovers are expected. However, they are not readily observed numerically because of the finite time step which produces a spurious propagation front which blurres such a crossover.

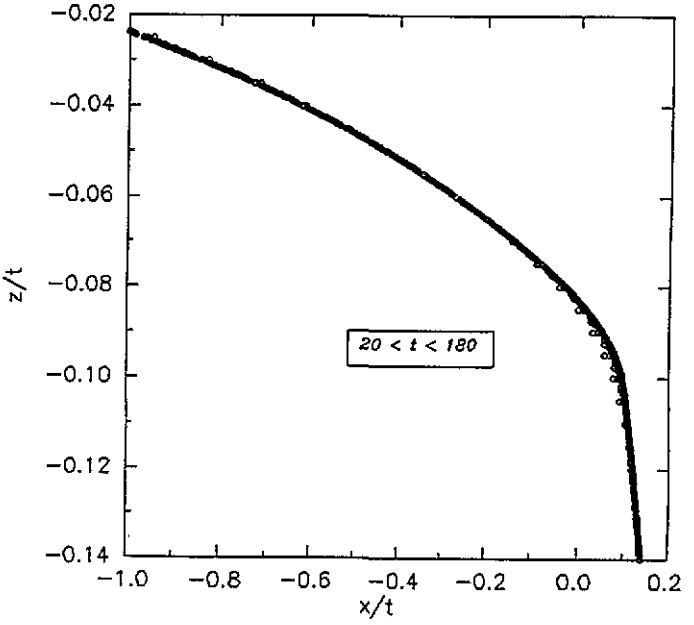


**Figure 5.** Self-similarity of profiles of a crystal without Schwoebel effect. The crossovers between the different regimes are blurred by numerical artifacts.

## 6. Grooves

In this section we consider the evaporation of a solid limited by a periodic array of grooves (figure 6($a$)). The sides of the grooves are assumed to be planar at the initial time $t = 0$. It is sufficient to study the evolution of a half period (figure 6($b$)), which contains a time-dependent number $n_{\max}(t)$ of steps. The origin $x = 0$ will be chosen at the highest point,

supposed to be the left-hand side of the half-period. The steps will be labelled $1, 2, \ldots, n_{max}$ from the left to the right.

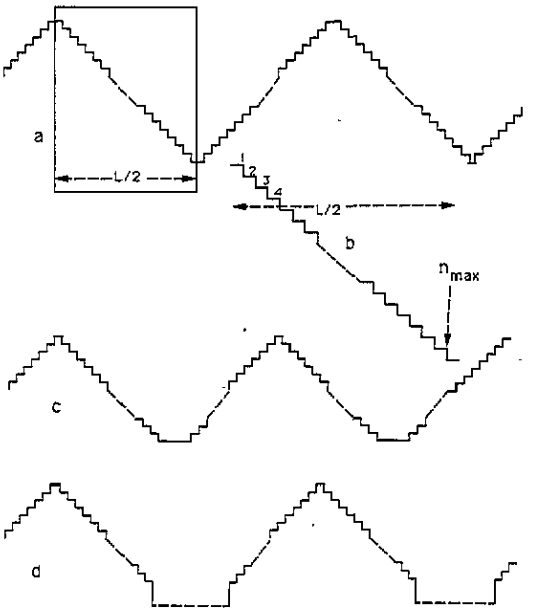


**Figure 6.** (*a*) Initial profile of the surface studied in section 6. (*b*) Enlargement of the half-period inside the rectangle of figure 6(*a*). (*c*) The evaporation shape as would be predicted in the continuum approximation. (*d*) The real shape resulting from step bunching, not taking into account the step pairing occasionally observed in simulations.

Only the symmetric case will be considered, so that the evolution of an isolated step is governed by equations (1.1) and (1.5). The two lowest steps of each period deserve special attention because they move in opposite directions, so that a facet appears at the lowest parts of the profile (figure 6(*c*)). Therefore, the position $n_{max}$ of the last step depends on time $t$.

It may be of interest to rewrite the equations of motion for the uppermost and the lowest steps as

$$\dot{x}_1 = -A\kappa\left[\tanh\left(\kappa\frac{x_2 - x_1}{2}\right) + \tanh(\kappa x_1)\right] \tag{6.1}$$

$$\dot{x}_{n_{max}} = -A\kappa\left[\tanh\left(\kappa\left(\frac{L}{2} + x_{n_{max}}\right)\right) + \tanh\left(\kappa\frac{x_{n_{max}} - x_{n_{max}-1}}{2}\right)\right] \tag{6.2}$$

where $L$ is the initial width of the groove. Two new features appear with respect to the evolution of the profile studied in the previous sections. On one hand, the highest step will disappear after some time, and at that time it is necessary to update the $x_n$'s and to replace $n_{max}$ by $n_{max} - 1$. A similar updating will take place every time $x_1$ vanishes, until the last step disappears and the surface becomes perfectly smooth. On the other hand, since a facet appears at the bottom, the first term at the right-hand side of equation (6.2) becomes large. Therefore, the lowest step moves faster than the other steps and, after some time, it reaches the step just above it. Evaporation generates step bunching! Step bunching is frequently observed after growing or annealing crystals, and various explanations have been proposed. The present one, though very simple, seems to be new.

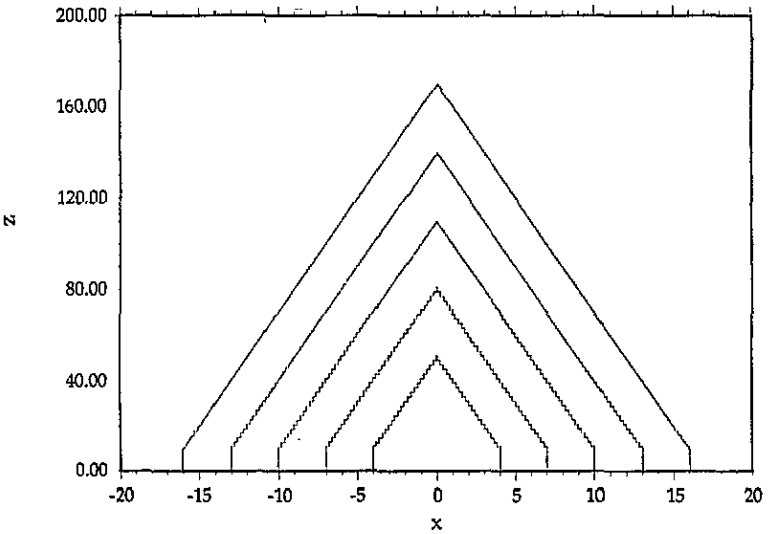


**Figure 7.** Snapshots of the evolution of the initial profile shown in figure 1(*a*). Profiles are drawn every ten time units defined in the text. Two different scales have been chosen in the axes, as explained in the text.

When the lowest step has reached the next one, equation (6.2) should be modified, because the step positions should satisfy the conditions $x_n > x_{n-1}$. The new equation may be found if one assumes, following BCF, that steps (whether forming bunches or not) are in equilibrium with the bulk. This results from the assumption that the motion of atoms along steps requires lower activation energies than atom detachment from steps. It follows that the chemical potential on the lowest terrace (the broad one) near a step should be the bulk chemical potential, and that the adatom density on the lowest terrace near a step should be the equilibrium adatom density, just as in the case of a single step. On the other hand, the adatom density $\rho(x)$ satisfies the diffusion equation (A.1) (see appendix) independently of the number $p$ of steps in the bunch which limits the lowest terrace. Since the boundary condition is also independent of $p$, $\rho(x)$ is independent of $p$. Therefore the current at the right-hand side of the lowest step, which is the gradient of $\rho$, is also independent of $p$, and therefore it is given by $\tanh(\kappa(L/2 - x_{n_{\max}}))$. On the other hand, the current to the left of the highest step in the lower bunch is $\tanh(\kappa(x_{n_{\max}-p} - x_{n_{\max}-p+1})/2)$ independently of $p$. There is a current of atoms inside the bunch, the effect of which is to maintain the chemical potential uniform within the bunch. It is seen that the current from the lowest step is larger than from the highest one. This ensures the stability of the bunch, i.e. its highest step does not move faster than the lowest one. Therefore all velocities within the bunch are the same:

$$\dot{x}_{n_{\max}} = -\frac{A\kappa}{p}\left[\tanh\left(\kappa\left(\frac{L}{2} - x_{n_{\max}}\right)\right) + \tanh\left(\kappa\frac{x_{n_{\max}-p} - x_{n_{\max}-p+1}}{2}\right)\right]. \tag{6.3}$$

If bunches of steps appear at places other than the bottom of the profile, equation (1.1) should be modified and replaced by an equation similar to (6.3). However, no large bunches have been observed in the numerical solution of the equations, so that the resulting profile is essentially the one represented in figure 6(*d*). If a bunch appears, it is necessary to check its stability. As said above, a bunch is stable if the current from its lowest step is larger than the current from its highest step. Thus, the condition for a bunch of $p$ steps to be

stable if its highest step is step $m$ is

$$\tanh\left(\kappa\frac{x_m - x_{m-1}}{2}\right) < \frac{1}{p-1}\tanh\left(\kappa\frac{x_{m+p+1} - x_{m+p}}{2}\right). \tag{6.4}$$

We have performed a numerical study of the evolution for the profile shown in figure 6($a$), with $l(0) = 0.1\kappa$. Initially, the highest and lowest terraces are twice as broad as the others. Figure 7 depicts the profile at different times during evaporation. The top of the profile remains linear while, at the bottom, a bunch appears as expected. At the beginning, this bunch grows, but, in our calculations, it reaches a maximal size after some time. This size is reached when the width of the lowest terrace becomes of order $1/\kappa$ so that further increase of that width does not produce a further increase of the current from the lowest step. Thus, according to (6.3) the velocity of the bunch is of order $1/p$. This velocity should be about the same as that of the next step, which is of order 1. Therefore, the number $p$ of steps in the bunch is given by $p = 1/(l(0)\kappa)$. After the bunch has reached its maximal size, the pairing of steps is observed. We explain the formation of a step pair just above the bottom bunch as follows. Immediately after reaching saturation, the bunch can have (because of the high $p$ value in equation (6.3)) a velocity smaller than the next step. Therefore, this step will move at a higher velocity than the others and will form a pair of steps with the next one. The formation of the other step pairs are presumably of similar origin. Step pairing is not always observed and depends on the initial conditions.

It is easily deduced from the above arguments that, if the initial width is larger than $1/\kappa$, no bunches are observed.

It is interesting to compare our results (figures 6 and 7) with what might be expected from the continuum approximation. For the sake of simplicity and because it corresponds to usual experiments, only the case $l \ll 1/\kappa$ will be addressed. Then, equation (2.5) reduces to

$$\dot{z} = A\kappa^2 \tag{6.5}$$

so that evaporation just translates the profile downwards. However, the lowest terrace does not evaporate, so that the resulting profile is essentially that of figure 6($c$). A similar conclusion would be obtained from Frank's construction. The continuum approximation fails to predict the bunches observed in figures 6($d$) and 7. As in the previous sections, the failure of the continuum approximation is related to the existence of angular points, namely those at the bottom of figure 6($c$). However, in the profile studied in the previous sections, the initial angular point became smooth, and therefore Frank's construction applied at later times; while in the sawtooth profile of figure 6, the angular points remain and even give rise to facets which are unexpected in the continuum approximation.

We have also studied the evolution of initially sinusoidal profiles or other differentiable profiles (figure 8($a$) and 8($b$)). The main new feature is that an angular point appears at the top if the upper terrace is broader than $1/\kappa$ (figure 8($a$)). The reason is the saturation effect associated with the hyperbolic tangent in (1.5): the top of the profile does not evaporate while the remainder of the surface follows equation (6.5). This angular point will nevertheless not be observed in most of real materials because large surface adlacunes (not taken into account in the present model) will be nucleated.

We have also made preliminary studies of the evolution of periodic profiles with the Schwoebel effect. The situation is rather complicated because of instabilities, reminiscent of those found by Kandel and Weeks [12] in a model combining an extreme Schwoebel effect, growth and impurities.

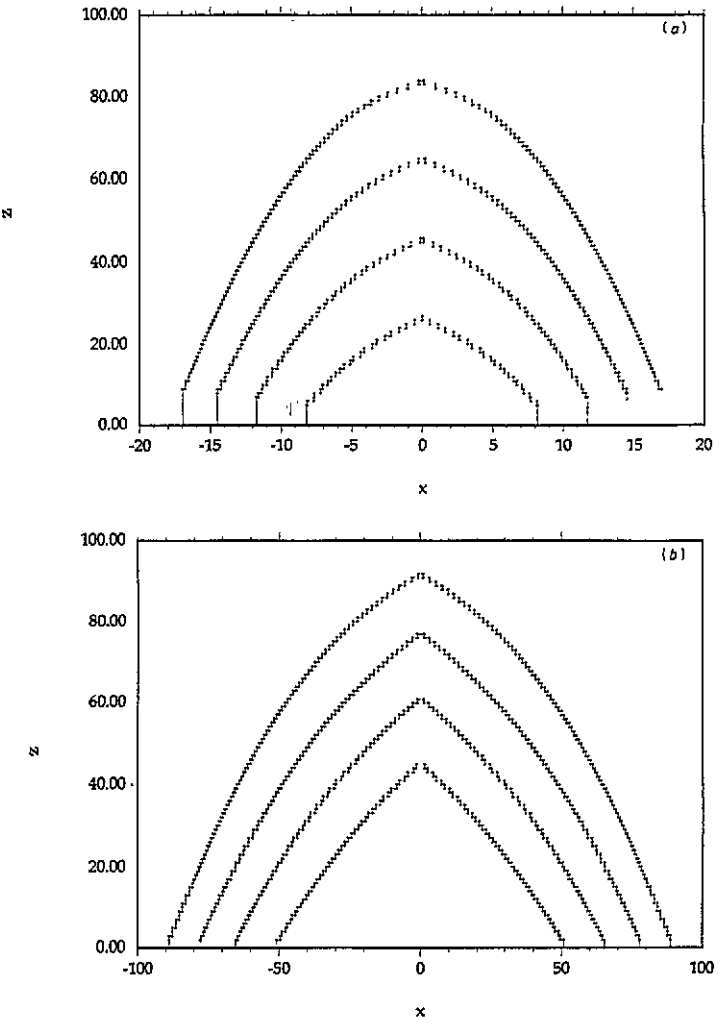


**Figure 8.** Snapshots of the evolution of an initial parabolic profile. (*a*) Evolution when initially all terraces are smaller than $1/\kappa$. (*b*) Evolution when initially the top terraces are larger than $1/\kappa$ and the bottom ones smaller than this value.

## 7. Conclusion

We have studied the evaporation of a crystal within the Burton–Cabrera–Frank model in two cases: (i) when the surface is limited by two planes, one of them having a high-symmetry orientation (figure 1(*a*)); (ii) for a 'grooved' surface (figure 6). We have paid attention to the Schwoebel effect (asymmetry of the sticking coefficient) and to the validity of Frank's theorem, based on the continuum approximation. However, we have not investigated cases where the instabilities described by Schwoebel [6] and by Kandel and Weeks [12] occur.

In the case of a corner (figure 1(*a*)), Frank's construction can only predict the evolution of the crystal above a particular plane $\Pi$, and below another plane $\Pi'$, but not between the two planes. Our numerical solution shows a rounding of the corner and an evolution of the profile towards a self-similar shape. We have also shown that the distance between upper ledges diverges logarithmically with time except in the case of a total normal Schwoebel

effect. This divergence wouldn't occur if the continuum approximation were exact. An approximate form of the equation of motion has also been investigated, which allows an exact solution.

In the case of a grooved surface, the bottom of the grooves is found to flatten, but their edges become steeper due to step bunching. The mechanism responsible for this effect is a very simple one; however, it cannot be deduced from the continuum approximation.

The present work can help to understand the formation of defects during annealing of crystal surfaces. However, direct comparison with experiment is not possible because, in the present work, steps are assumed to be straight, and dislocations are neglected. This is only correct for small length scales, usually around 0.01 cm or less. We have also ignored the effect of vacancies, which are certainly important near the melting point of elements [9], and can even suppress the saturation effect appearing in formula (1.5) when $\kappa l > 1$. Note that this saturation effect has been observed experimentally in some materials, as for example did Keller in NaCl [13]. Neglecting vacancies is only correct if terrace sizes are small. A quantitative discussion has been given in [14].

It is interesting to compare our results with those reported by Stoyanov [8] for a stepped surface in which an external force acts on the adatoms. In that case, bunch formation is predicted when $\Psi(l) \equiv \varphi_r(l) - \varphi_l(l)$ is positive for a terrace wider than its neighbouring terraces, of width $l$. The sign of $\Psi(l)$ depends on the direction of the external force. In our case, for an initial surface given by figure 1(*a*), $\Psi(l)$ is positive in the case of inverse Schwoebel effect. Bunches have not been observed because they will develop above the terrace which is larger than its neighbouring ones. In our case, these would correspond to terraces on the top of our first terrace and have not been considered in the analysis. As regards bunch formation in grooves, it is observed even in the symmetric case, although $\varphi_r(l) = \varphi_l(l)$, because $\Psi(l)$ is always positive for the terrace at the bottom.

**Acknowledgments**

One of the authors (IP) wants to thank Ministerio de Educación y Ciencia for financial support.

## Appendix A. Velocity of the steps with Schwoebel effect

In this appendix we derive the expression for the step velocity as sketched in section 1. If the diffusion process of adatoms on the surface is much faster than the motion of steps, as supposed by BCF [3], the adatoms reach a stationary state during the motion of the steps and the velocity of the step is related to the flux of such an adatom density. Then, we should determine the density profile on the terraces in order to calculate the step velocity.

Between two steps, the adatom density $\rho_n(x)$ satisfies the following equation:

$$\frac{\partial \rho_n(x)}{\partial t} = D\frac{\partial^2 \rho_n(x)}{\partial x^2} - \frac{1}{\tau_0}\rho_n(x) + F \qquad x_n < x < x_{n+1} \tag{A.1}$$

where the first term on the right-hand side corresponds to diffusion, the second one to evaporation and the third one to deposition. In the present article, $F$ is taken to be zero.

The boundary conditions at the steps are the following ones, which state the equality of

two expressions of the current density $j(x)$:

$$-j(x) = D\frac{\partial \rho_n(x)}{\partial x} = D''\rho_0 - D''\rho_n(x) \qquad (x = x_n - \epsilon) \tag{A.2}$$

$$-j(x) = D\frac{\partial \rho_n(x)}{\partial x} = D'\rho_0 - D'\rho_n(x) \qquad (x = x_{n-1} + \epsilon) \tag{A.3}$$

where $\epsilon$ denotes a small quantity. $D'\rho_0$ and $D''\rho_0$ are the current of adatoms detaching from both sides of the step. These values are imposed by detailed balance.

Diffusion is usually much faster than step motion, so that the left-hand side of (A.1) may be replaced by zero. It is then straightforward to calculate $\rho_n(x)$, and to deduce the current density on both sides of each step using equations (A.2) and (A.3), which are precisely $\varphi_l$ and $\varphi_r$. Equations (1.2) and (1.3) are therefore easily deduced after some algebra.

When $l$ is large, the second-order expansion of (1.2) and (1.3) in powers of $\exp(-\kappa l)$ is given by equations (3.1) and (3.2), where

$$\Delta = \frac{(\rho_0 - F\tau_0)\kappa D}{1 + \frac{\kappa^2 D^2}{D'D''} + \frac{\kappa D}{D'} + \frac{\kappa D}{D''}} \tag{A.4}$$

$$A' = 1 + \frac{\kappa D}{D'} \tag{A.5}$$

$$C' = 1 - \frac{\kappa D}{D'} - \left(1 + \frac{\kappa D}{D'}\right)\frac{\frac{\kappa D}{D'} + \frac{\kappa D}{D''} - 1 - \frac{\kappa^2 D^2}{D'D''}}{1 + \frac{\kappa^2 D^2}{D'D''} + \frac{\kappa D}{D'} + \frac{\kappa D}{D''}} \tag{A.6}$$

and $A''$ and $C''$ are obtained by interchanging $D'$ and $D''$ in (A.5) and (A.6), respectively.

## Appendix B. Short-time symmetric case profile

In this appendix we derive equations (4.5), starting from the approximate terrace-width evolution equations (4.4). Using vector notation these are rewritten in the more convenient form

$$|\dot{l}(t)\rangle = \tfrac{1}{2}A\kappa^2 Y|l(t)\rangle + A\kappa|1\rangle \tag{B.1}$$

with the vector $|\dot{l}(t)\rangle$ being

$$|\dot{l}(t)\rangle = \begin{pmatrix} l_1(t) \\ l_2(t) \\ \vdots \\ l_n(t) \\ \vdots \\ l_N(t) \end{pmatrix} \tag{B.2}$$

and where we have introduced

$$Y = \begin{pmatrix} 0 & -1 & 0 & 0 & 0 & \dots \\ 1 & 0 & -1 & 0 & 0 & \dots \\ 0 & 1 & 0 & -1 & 0 & \dots \\ 0 & 0 & 1 & 0 & -1 & \dots \\ 0 & 0 & 0 & 1 & 0 & \dots \\ \dots & \dots & \dots & \dots & \dots & \dots \end{pmatrix} \qquad \text{and} \qquad |1\rangle = \begin{pmatrix} 1 \\ 0 \\ 0 \\ 0 \\ 0 \\ \dots \end{pmatrix}. \tag{B.3}$$

The formal solution of (B.1) is easily checked to be

$$|l(t)\rangle = e^{\Omega t}\left(|l(0)\rangle + 2\kappa^{-1}Y^{-1}|1\rangle\right) - \frac{2}{\kappa}Y^{-1}|1\rangle \tag{B.4}$$

with $\Omega = \frac{1}{2}A\kappa^2 Y$.

In order to find an explicit solution to equation (B.4), we should decompose the matrix $Y$ in eigenvectors, so that the exponential $e^{\Omega t}$ can be diagonalized. To this end, we introduce the vectors

$$\langle k| = \left( 1, \quad e^{-ik}, \quad e^{-2ik}, \quad \ldots, \quad e^{-ink}, \quad \ldots, \quad e^{-iNk} \right) \tag{B.5}$$

with $n$ a natural number, $n = 0, 1, \ldots, N$. We can now construct the eigenvectors of $Y$, which is a finite Toeplitz matrix, as an appropriate combination of $|k\rangle$. It is readily checked that

$$|k) \equiv \frac{1}{\sqrt{2N}} \left( e^{ik}|k) + e^{-ik}|\pi - k) \right) \tag{B.6}$$

are such vectors if $N$ is an odd number, and $k$ takes the values $k = \frac{(2j-1)\pi}{2(N+1)}$, $j = -N, \ldots, N+1$. The corresponding eigenvalues are $-2i\sin(k)$. Then, the exponential, in terms of these eigenvectors, has the form

$$e^{\frac{1}{2}A\kappa^2 tY} = \sum_k e^{-iA\kappa^2 t \sin(k)} |k)(k|. \tag{B.7}$$

We should now express the exponential in real space. To this end, we have to evaluate the action of the operator on vectors $|n\rangle$, which has its $n$th component equal to 1, and the rest of them equal to zero. Using the fact that

$$\langle n|k) = \frac{1}{\sqrt{2N}} \left( e^{ink} + (-1)^{n-1} e^{-ink} \right) \tag{B.8}$$

one can determine the value of the exponential acting on such vectors

$$\begin{aligned} \langle n|e^{\frac{1}{2}A\kappa^2 tY}|m\rangle &= \sum_k e^{-iA\kappa^2 t \sin(k)} \langle n|k)(k|m\rangle \\ &= \frac{1}{2N} \sum_k e^{-iA\kappa^2 t \sin(k)} \left( e^{-ink} + (-1)^{n-1} e^{ink} \right) \left( e^{imk} + (-1)^{m-1} e^{-imk} \right). \end{aligned} \tag{B.9}$$

As we are interested in the situation where there is a large number of terraces, and then the behaviour of the system will not be very sensitive on the specific value of N, which is large, one can approximate the sums in equation (B.9) by integrals

$$\begin{aligned} \langle n|e^{\frac{1}{2}A\kappa^2 tY}|m\rangle = \frac{1}{2\pi} \int_{-\pi/2}^{\pi/2} dk\, e^{-iA\kappa^2 t \sin(k)} \big( & e^{i(m-n)k} + (-1)^{(n+m)} e^{i(n-m)k} \\ & + (-1)^{(m+1)} e^{-i(m+n)k} + (-1)^{(n+1)} e^{i(m+n)k} \big). \end{aligned} \tag{B.10}$$

Then, using the equality

$$\frac{1}{2\pi} \int_{-\pi/2}^{\pi/2} dk\, e^{-iA\kappa^2 t \sin(k)} \left( e^{ipk} + (-1)^p e^{-ipk} \right) = J_p(-A\kappa^2 t) \tag{B.11}$$

with $J_n(x)$ being the Bessel function of order $n$, one determines the value of equation (B.10), namely

$$\langle n| \exp(A\kappa^2 tY/2)|m\rangle = J_{n-m}(A\kappa^2 t) + (-1)^{m+1} J_{n+m}(A\kappa^2 t) \tag{B.12}$$

which enables us to write down the expression of the exponential in real space

$$\exp(A\kappa^2 tY/2) = \begin{pmatrix} J_0 + J_2 & -J_1 - J_3 & J_2 + J_4 & -J_3 - J_5 & \ldots & \ldots \\ J_1 + J_3 & J_0 - J_4 & -J_1 + J_5 & J_2 - J_6 & \ldots & \ldots \\ J_2 + J_4 & J_1 - J_5 & J_0 + J_6 & -J_1 - J_7 & \ldots & \ldots \\ J_3 + J_5 & J_2 - J_6 & J_1 + J_7 & J_0 - J_8 & \ldots & \ldots \\ \ldots & \ldots & \ldots & \ldots & \ldots & \end{pmatrix} \tag{B.13}$$

where all the Bessel functions have an argument equal to $A\kappa^2 t$.

On the other hand, when applying $Y$ on $|l(t)\rangle$, the formal solution (B.4) is expressed by

$$\begin{pmatrix} -l_2(t) \\ l_1(t) - l_3(t) \\ l_2(t) - l_4(t) \\ \cdots \end{pmatrix} = \exp(A\kappa^2 tY/2) \left( \begin{pmatrix} -l(0) \\ 0 \\ 0 \\ \cdots \end{pmatrix} + 2\kappa^{-1}|\psi\rangle \right) - 2\kappa^{-1}|\psi\rangle. \tag{B.14}$$

Now, applying expression (B.13) for the matrix to equation (B.14), we finally arrive at expressions (4.5) for the terrace widths as a function of time and the number of the terrace, once the initial terrace width is known.

## References


[1] Alfonso C, Bermond J M, Heyraud J C and Métois J J 1992 *Surf. Sci.* **262** 371
[2] Latyshev A V 1989 *Surface Sci.* **213** 157
[3] Burton W K, Cabrera N and Frank F 1951 *Phil. Trans. R. Soc.* **243** 299
[4] Frank F C 1958 *Growth and perfection of crystals* (New York: Wiley) p 411
[5] Ehrlich G and Hudda F G 1966 *J. Chem. Phys.* **44** 1039
[6] Schwoebel R L 1969 *J. Appl. Phys.* **40** 614
[7] Bales and Zangwill 1990 *Phys. Rev.* B **41** 5500
[8] Stoyanov S 1991 *Jap. J. Appl. Phys.* **30** 1
[9] Mundschau M, Bauer E, Telieps W and Swiech W 1989 *Surf. Sci.* **223** 413
[10] Metois J J *et al* private communication
[11] Press W A, Flannery B P, Teukolsky S A and Vetterling W T 1986 *Numerical Recipes* (Cambridge: Cambridge University Press)
[12] Kandel D and Weeks J D 1992 *Phys. Rev. Lett.* **69** 3758
[13] Keller K W *Crystal Growth and Characterization* ed R Ueda and J B Mullin (Amsterdam: North Holland)
[14] Pimpinelli A and Villain J 1994 *Physica* (to be published)